

# Can we swim in superfluids?: Numerical demonstration of self-propulsion in a Bose-Einstein condensate

Hiroki Saito

*Department of Engineering Science, University of Electro-Communications, Tokyo 182-8585, Japan*

It is numerically investigated whether a deformable object can propel itself in a superfluid. Articulated bodies and multi-component condensates are examined as swimmers. An articulated two-body swimmer cannot obtain locomotion without emitting excitations. More flexible swimmers can do so without the need to excite waves.

## 1. Introduction

Superfluids have no viscosity. When an object is moved in a superfluid at a subcritical constant velocity, it experiences no drag force. It would seem, therefore, that the arms and legs of a swimmer will be unable to generate propulsion in a superfluid. Can we swim in such a fluid? In other words, is the self-propulsion of a deformable object in a superfluid possible?

The present paper shows that the answer to this question is yes. Let us first consider a case in which the velocity of the flow around the swimmer is much slower than the velocity of sound. In this case, a superfluid may be regarded as an incompressible ideal fluid. Several authors have shown that the self-propulsion of a deformable body is possible even in an incompressible ideal fluid,<sup>1–5</sup> and therefore, we expect that self-propulsion is also possible in a superfluid. When the swimmer deforms quickly, on the other hand, the superfluid cannot be regarded as incompressible, and waves and quantized vortices are generated. Since these excitations are able to carry momentum, the swimmer can obtain thrust by releasing them. The aim of the present paper is to verify these speculations.

The dynamics of objects immersed in superfluids have been studied in various situations, such as using particles to visualize superfluid flow,<sup>6,7</sup> using oscillating spheres<sup>8</sup> and wires<sup>9</sup> to disturb superfluid helium, and considering the behavior of an ion<sup>10</sup> in a gaseous Bose-Einstein condensate (BEC). However, the self-propulsion of an object in a superfluid has not been studied.

In the present paper, we use the mean-field Gross-Pitaevskii (GP) theory to numerically demonstrate that deformable objects can swim in a two-dimensional (2D) superfluid. Two kinds of swimmers are examined: articulated bodies with movable joints and multicomponent BECs. For the latter type, the swimmer is also a BEC and can be deformed by changing the interactions between atoms. Since a superfluid has no viscosity, one may think that the swimmer would behave as if it had a high Reynolds number. However, the condition for self-propulsion in a superfluid is shown to be similar to that for a swimmer with a low Reynolds number in a viscous fluid;

this is reminiscent of Purcell's "scallop theorem".<sup>11</sup>

This paper is organized as follows. Section 2 investigates the dynamics of articulated bodies in a BEC. Section 3 studies the dynamics of multicomponent BECs. Section 4 presents the conclusions of our study.

## 2. Articulated bodies in a superfluid

We consider the dynamics of a superfluid of atoms with mass  $m$  in the mean-field approximation. The dynamics of the macroscopic wave function  $\psi$  are described by the GP equation

$$i\hbar \frac{\partial \psi}{\partial t} = -\frac{\hbar^2}{2m} \nabla^2 \psi + V\psi + g|\psi|^2\psi, \quad (1)$$

where  $V$  is the potential produced by a swimmer. For simplicity, we will consider a 2D space, which can be realized by tightly confining the system in the  $z$  direction. Assuming the form of the wave function is  $\psi_{3D}(x, y, z) = \psi(x, y)\phi(z)$ , the effective interaction coefficient  $g$  in Eq. (1) is given by  $g = 4\pi\hbar^2 a \int |\phi|^4 dz / m$ , where  $a$  is the  $s$ -wave scattering length.

In this section, we consider swimmers that consist of elliptic bodies, as illustrated in Fig. 1. The elliptic bodies are connected at joints located on the long axes of the ellipses. The distance between the centers of the ellipses and the joints is  $d$ . The angles  $\chi$  of the joints are controlled variables. To reduce numerical errors arising from the rigid boundary condition at the surface of the bodies, a "soft" boundary condition is adopted. For the  $j$ th elliptic body centered at  $(x_j, y_j)$  and for which the angle between its long axis and the  $x$  axis is  $\theta_j$ , the potential is given by

$$v_j(x, y) = \mu_0 \exp\{f_{\text{pot}}[1 - (\xi_j/\alpha)^2 - (\eta_j/\beta)^2]\}, \quad (2)$$

where  $\xi_j = (x - x_j) \cos \theta_j + (y - y_j) \sin \theta_j$ ,  $\eta_j = -(x - x_j) \sin \theta_j + (y - y_j) \cos \theta_j$ , and  $\mu_0$  is the chemical potential far from the swimmer. The potential in Eq. (2) is  $v_j = \mu_0$  at an ellipse  $(\xi_j/\alpha)^2 + (\eta_j/\beta)^2 = 1$ , which corresponds to the surface of the body. The parameter  $f_{\text{pot}}$  in Eq. (2) determines the sharpness of the surface; the Gaussian potential rises steeply for a large  $f_{\text{pot}}$ . The results are insensitive to the value of  $f_{\text{pot}}$ , and we set  $f_{\text{pot}} = 1$  in the following calculations. The potential  $V$  in the

GP equation is thus given by

$$V(x, y) = \sum_j v_j(x, y). \quad (3)$$

The Lagrangian for the swimmer is given by

$$L = \sum_j \left[ \frac{M}{2} (\dot{x}_j^2 + \dot{y}_j^2) + \frac{I}{2} \dot{\theta}_j^2 \right] - U_{\text{pot}}(X, Y, \theta, \chi; \psi), \quad (4)$$

where  $M$  and  $I$  are the mass and the moment of inertia of the elliptic body, respectively. The interaction potential  $U_{\text{pot}}$  between the swimmer and superfluid has the form

$$U_{\text{pot}}(X, Y, \theta, \chi; \psi) = \int V|\psi|^2 dr, \quad (5)$$

where  $(X, Y)$  are coordinates of the center of mass (COM) of the swimmer. The potential  $V$  depends on  $(X, Y)$ ,  $\theta$ , and  $\chi$ , through Eq. (2). In the following, we assume  $M = \pi\alpha\beta mn_0$  and  $I = M(\alpha^2 + \beta^2)/4$ , where  $n_0$  is the density far from the swimmer.

Equation (1) and the equation of motion for the swimmer are solved numerically, using the pseudospectral and fourth-order Runge-Kutta methods. The initial state of  $\psi$  is prepared by the imaginary-time propagation method, in which the swimmer is at rest in the initial form. The density  $|\psi|^2$  far from the swimmer is constant  $n_0$ , which gives the characteristic length  $\xi = \hbar/(mg n_0)^{1/2}$  and time  $\tau = \xi/v_s$ , where  $v_s = (g n_0/m)^{1/2}$  is the velocity of sound. The following quantities are fixed:  $\alpha = 5\xi$ ,  $\beta = \xi$ , and  $d = 7\xi$ . A periodic boundary condition is imposed by the pseudospectral method. The numerical space is taken to be sufficiently wide, and the boundary does not affect the results if the motion of the swimmer is moderate. In this case, the total momentum of the swimmer and surrounding fluid is conserved. When the swimmer moves violently, waves and vortices are released, and these reach the boundary. In that case, an artificial damping term  $-\Gamma(\mathbf{r})\hbar\partial\psi/\partial t$  is added to the left-hand side of Eq. (1), where  $\Gamma(\mathbf{r})$  is nonzero only near the boundary.<sup>12</sup> The artificial damping term can suppress the disturbances at the boundary without affecting the dynamics of the swimmer.

### 2.1 Two-body swimmer

We begin by considering a swimmer created from two elliptic bodies connected by a joint, as shown in Fig. 1(a). The state of the swimmer is specified by the COM coordinate  $(X, Y)$ , direction  $\theta$  of the symmetry axis, and their time derivatives  $(\dot{X}, \dot{Y})$ ,  $\dot{\theta}$ . The angle  $\chi_1$  is the controlled variable, and the shape of the swimmer has only one degree of freedom.

For the two-body swimmer, the Lagrangian in Eq. (4) is rewritten as

$$L = M(\dot{X}^2 + \dot{Y}^2) + \frac{Md^2}{2} [\dot{\theta}^2 + \dot{\chi}_1^2 - (\dot{\theta}^2 - \dot{\chi}_1^2) \cos 2\chi_1] + I(\dot{\theta}^2 + \dot{\chi}_1^2) - U_{\text{pot}}(X, Y, \theta, \chi_1; \psi). \quad (6)$$

The dynamics of the swimmer are thus described by the Euler-

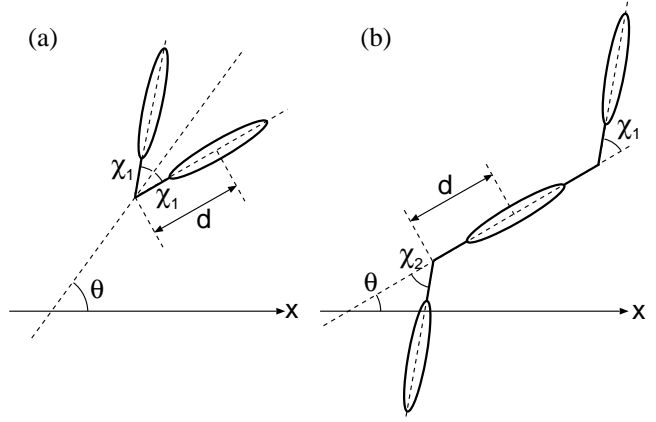


**Fig. 1.** Schematic illustration of the two-body and three-body swimmers used in Secs. 2.1 and 2.2, respectively. The distance  $d$  is constant between the center of the elliptic bodies and the joints. The angles  $\chi_1$  and  $\chi_2$  are controlled parameters.

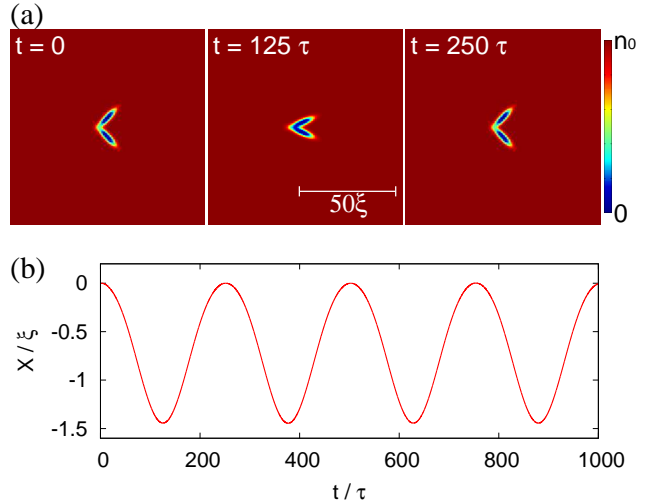


**Fig. 2.** (Color online) Time evolution of (a) the density profile  $|\psi|^2$ , and (b) the position  $X$  of the COM. The angle  $\chi_1(t)$  is driven as in Eq. (8) with  $A = \pi/4$  and  $\omega = 0.025\tau^{-1}$ . The length and time are normalized by the healing length  $\xi$  and  $\tau = \xi/v_s$ , where  $v_s$  is the sound velocity. See the Supplemental Material for a movie of the dynamics shown in (a).<sup>14</sup>

Lagrange equations,

$$2M\ddot{X} = -\frac{\partial U_{\text{pot}}}{\partial X}, \quad (7a)$$

$$2M\ddot{Y} = -\frac{\partial U_{\text{pot}}}{\partial Y}, \quad (7b)$$

$$[Md^2(1 - \cos 2\chi_1) + 2I]\ddot{\theta} = -\frac{\partial U_{\text{pot}}}{\partial \theta} - 2Md^2\dot{\theta}\dot{\chi}_1 \sin 2\chi_1. \quad (7c)$$

Equations (1) and (7) determine the dynamics of the system.

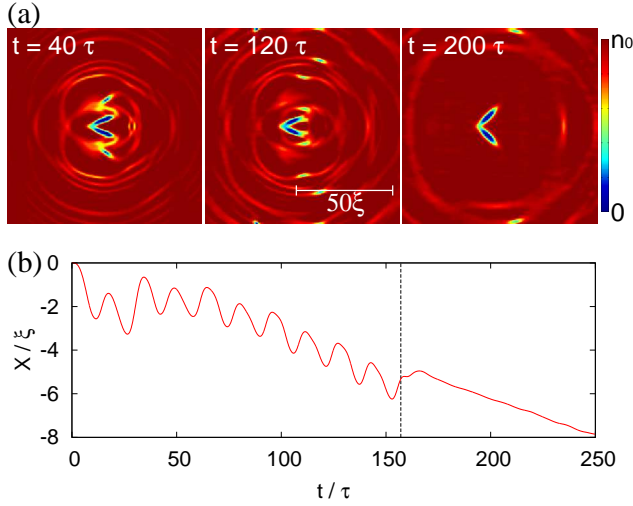


**Fig. 3.** (Color online) Time evolution of (a) the density profile  $|\psi|^2$ , and (b) the position  $X$  of the COM for  $\omega = 0.4\tau^{-1}$ . The angle  $\chi_1(t)$  is driven as in Eq. (8) for  $\omega t < 20\pi$ , and  $\chi_1(t) = 0$  for  $\omega t > 20\pi$ . The dashed line in (b) indicates  $\omega t = 20\pi$ . See the Supplemental Material for a movie of the dynamics shown in (a).<sup>16</sup>

First, we show that such an object cannot generate locomotion when it is deformed slowly. The swimmer is deformed periodically as

$$\chi_1(t) = A \left( 1 - \frac{1}{2} \sin^2 \frac{\omega t}{2} \right), \quad (8)$$

where  $A/2$  is the amplitude and  $\omega$  is a frequency of the oscillation. Figure 2 shows the time evolution of the system for  $A = \pi/4$  and  $\omega = 0.025\tau^{-1}$ . The swimmer is initially formed by two elliptic bodies that are joined at an angle  $\pi/2$ , and then it closes and opens periodically, as shown in Fig. 2(a). We can see in Fig. 2(b) that the action of the swimmer generates no net locomotion, whereas the position  $X$  of the COM moves back and forth at a frequency  $\omega$ , while conserving the total momentum.

The fact that the swimmer cannot propel itself in Fig. 2 reminds us of Purcell's "scallop theorem",<sup>11</sup> which states that when the motion of a swimmer has time-reversal symmetry,<sup>13</sup> there is no net locomotion of the swimmer in a viscous Stokes fluid. The periodic motion in Eq. (8) has time-reversal symmetry, and therefore the swimmer cannot swim in a Stokes fluid. Reference 15 showed that the scallop theorem can be generalized to a perfect fluid, i.e., a periodic motion with time reversal symmetry never generates locomotion in a perfect fluid. When the motion of the swimmer is sufficiently slow, and no waves or quantized vortices are excited, a superfluid can be regarded as a perfect fluid. The generalized scallop theorem is therefore applicable to the situation shown in Fig. 2. Thus, self-propulsion in a superfluid is impossible for a two-body swimmer with sufficiently slow deformation.

In the dynamics shown in Fig. 2, the typical velocity of

the elliptic bodies is  $\omega d = 0.175v_s$ , and this is much smaller than the velocity of sound  $v_s$ ; thus, the fluid around the swimmer is barely disturbed. When the swimmer is deformed more quickly, on the other hand, waves and quantized vortices are created, and the condensate can no longer be regarded as a perfect fluid; the generalized scallop theorem is no longer applicable. Figure 3 shows the dynamics of the system for  $\omega = 0.4\tau^{-1}$ , which is 16 times larger than the value used for Fig. 2. In this case, the shape of the swimmer changes faster than the sound velocity, and waves and solitonic pulses<sup>17,18</sup> are emitted from the swimmer, as shown in Fig. 3(a). By disturbing the fluid, the swimmer gains net locomotion, as shown in Fig. 3(b). At  $\omega t = 20\pi$  [the vertical dashed line in Fig. 3(b)], i.e., after ten strokes, the deformation of the swimmer is stopped:  $\chi_1(t) = 0$  for  $\omega t > 20\pi$ . Even after that, the swimmer continues to travel, which indicates that the swimmer acquires momentum by emitting waves and solitonic excitations into the surrounding fluid.

## 2.2 Three-body swimmer

We next study the dynamics of a swimmer consisting of three elliptic bodies connected by two joints, as illustrated in Fig. 1(b). The Lagrangian in Eq. (4) can be written as

$$\begin{aligned} L = & \frac{3M}{2}(\dot{X}^2 + \dot{Y}^2) + \frac{Md^2}{3}[(\dot{\theta} + \dot{\chi}_1)^2 + (\dot{\theta} + \dot{\chi}_2)^2 \\ & + (\dot{\theta} + \dot{\chi}_1)(\dot{\theta} + \dot{\chi}_2)\cos(\chi_1 - \chi_2) + 3\dot{\theta}(\dot{\theta} + \dot{\chi}_1)\cos\chi_1 \\ & + 3\dot{\theta}(\dot{\theta} + \dot{\chi}_2)\cos\chi_2 + 3\dot{\theta}^2] \\ & + \frac{I}{2}[\dot{\theta}^2 + (\dot{\theta} + \dot{\chi}_1)^2 + (\dot{\theta} + \dot{\chi}_2)^2] \\ & - U_{\text{pot}}(X, Y, \theta, \chi_1, \chi_2; \psi), \end{aligned} \quad (9)$$

which gives the Euler-Lagrange equations,

$$3M\ddot{X} = -\frac{\partial U_{\text{pot}}}{\partial X}, \quad (10a)$$

$$3M\ddot{Y} = -\frac{\partial U_{\text{pot}}}{\partial Y}, \quad (10b)$$

$$\begin{aligned} \ddot{\theta} = & \left\{ -\frac{\partial U_{\text{pot}}}{\partial \theta} - \frac{Md^2}{3}[(\ddot{\chi}_1 + \ddot{\chi}_2)(2 + \cos(\chi_1 - \chi_2)) \right. \\ & - (2\dot{\theta} + \dot{\chi}_1 + \dot{\chi}_2)(\dot{\chi}_1 - \dot{\chi}_2)\sin(\chi_1 - \chi_2) \\ & + 3\ddot{\chi}_1\cos\chi_1 + 3\ddot{\chi}_2\cos\chi_2 - 3(2\dot{\theta} + \dot{\chi}_1)\dot{\chi}_1\sin\chi_1 \\ & \left. - 3(2\dot{\theta} + \dot{\chi}_2)\dot{\chi}_2\sin\chi_2] - I(\ddot{\chi}_1 + \ddot{\chi}_2) \right\} \\ & / \left\{ \frac{2Md^2}{3}[5 + \cos(\chi_1 - \chi_2) + 3\cos\chi_1 \right. \\ & \left. + 3\cos\chi_2] + 3I \right\}. \end{aligned} \quad (10c)$$

There are two controlled parameters  $(\chi_1, \chi_2)$  that are used to specify the shape of the swimmer. When the periodic motion

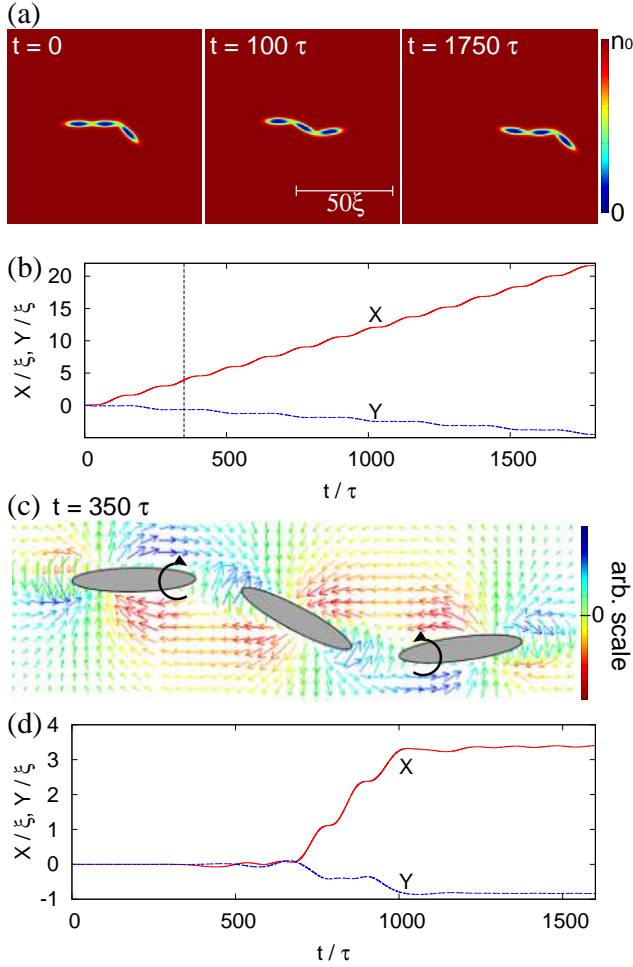


**Fig. 4.** (Color online) Time evolution of (a) the density profile  $|\psi|^2$ , and (b) the position of the COM of a three-body swimmer driven as in Eq. (11), with  $A = \pi/4$  and  $\gamma = \omega = 0.025\tau^{-1}$ . See the Supplemental Material for a movie of the dynamics in (a).<sup>19</sup> The vertical line in (b) indicates  $t = 350\tau$ . (c) Flow field  $\mathbf{J}$  at  $t = 350\tau$ . The length of the vector is proportional to  $|\mathbf{J}|$ , and the color represents  $J_x$ . The black arrows indicate the directions in which the joints are rotating. (d) Time evolution of the position of the COM of the three-body swimmer driven as in Eq. (13), with  $A = \pi/4$ ,  $\gamma = 2 \times 10^{-5}\tau^{-2}$ ,  $t_0 = 800\tau$ , and  $\omega = 0.025\tau^{-1}$ .

of the swimmer is represented by a closed loop in  $(\chi_1, \chi_2)$  space, the motion is neither time-reversal symmetric nor reciprocal,<sup>13</sup> and therefore, locomotion is not prohibited by the generalized scallop theorem.

Figures 4(a) and 4(b) show the dynamics of the three-body swimmer for

$$\chi_1(t) = -A \left( 1 - 2 \tanh \gamma t \sin^2 \frac{\omega t}{2} \right), \quad (11a)$$

$$\chi_2(t) = A \tanh \gamma t \sin \omega t, \quad (11b)$$

where  $A = \pi/4$  and  $\gamma = \omega = 0.025\tau^{-1}$ . The factor  $\tanh \gamma t$  is introduced to avoid infinite acceleration of the body at  $t = 0$ . For  $t \gg \gamma^{-1}$ , Eq. (11) reduces to  $\chi_1(t) \simeq -\cos \omega t$  and  $\chi_2(t) \simeq$

$\sin \omega t$ . Since the trajectories of  $\chi_1(t)$  and  $\chi_2(t)$  are circles in  $(\chi_1, \chi_2)$  space, net locomotion is allowed. We can see from Figs. 4(a) and 4(b) that the three-body swimmer propels itself without exciting waves or vortices, in contrast to the two-body swimmer. The three-body swimmer travels by  $\simeq 3\xi$  for each stroke cycle.

Intuitive understanding of self-propulsion is difficult, because the flow field

$$\mathbf{J} = \frac{\hbar}{2mi} (\psi^* \nabla \psi - \psi \nabla \psi^*) \quad (12)$$

around the three-body swimmer is complicated, as shown in Fig. 4(c). At  $t = 350\tau$ , the position  $X$  of the COM of the swimmer is increasing [vertical line in Fig. 4(b)], and hence the superfluid should have a momentum in the  $-x$  direction, due to conservation of the total momentum. The red (light gray) region in Fig. 4(c) has a large momentum in the  $-x$  direction, and this plays an important role in the locomotion of the swimmer.

Figure 4(d) shows the position of the COM for swimmer's shape given by

$$\chi_1(t) = A \left( 1 - 2e^{-\gamma(t-t_0)^2} \sin^2 \frac{\omega t}{2} \right), \quad (13a)$$

$$\chi_2(t) = Ae^{-\gamma(t-t_0)^2} \sin \gamma t, \quad (13b)$$

where  $A = \pi/4$ ,  $\gamma = 2 \times 10^{-5}\tau^{-2}$ ,  $t_0 = 800\tau$ , and  $\omega = 0.025\tau^{-1}$ . These functions begin at  $\chi_1(0) \simeq \pi/4$  and  $\chi_2(0) \simeq 0$ , oscillate while  $t/\tau \simeq 800 \pm 300$ , and stop at  $\chi_1(\infty) = \pi/4$  and  $\chi_2(\infty) = 0$ . In this case, the swimmer travels only during the deformation, and the locomotion nearly stops after the shape stops changing. This behavior is also similar to the self-propulsion of a swimmer in a viscous Stokes fluid. The small fluctuations of  $X$  and  $Y$  for  $t/\tau \gtrsim 1200$ , shown in Fig. 4(d), are due to a non-adiabatic disturbance of the condensate. They vanish when the deformation of the swimmer is sufficiently slow.

### 3. Swimming in multicomponent condensates

We next consider the dynamics of a multicomponent BEC, in which there is a swimmer who also consists of BECs of different components. We will consider an immiscible three-component BEC. Suppose that a swimmer of components 1 and 2 is surrounded by a sea of component 3. By controlling the scattering lengths by using the Feshbach resonance, the size of the droplets of components 1 and 2 can be changed, that is, the shape of the swimmer can be controlled.

The dynamics of the system can be studied by numerically solving the GP equation for a three-component BEC

$$i\hbar \frac{\partial \psi_j}{\partial t} = -\frac{\hbar^2}{2m} \nabla^2 \psi_j + \sum_{k=1}^3 g_{jk} |\psi_k|^2 \psi_j, \quad (14)$$

where  $j = 1, 2$ , and 3. The interaction coefficients  $g_{jk}$  depend on time in such a way that they always satisfy the immiscible

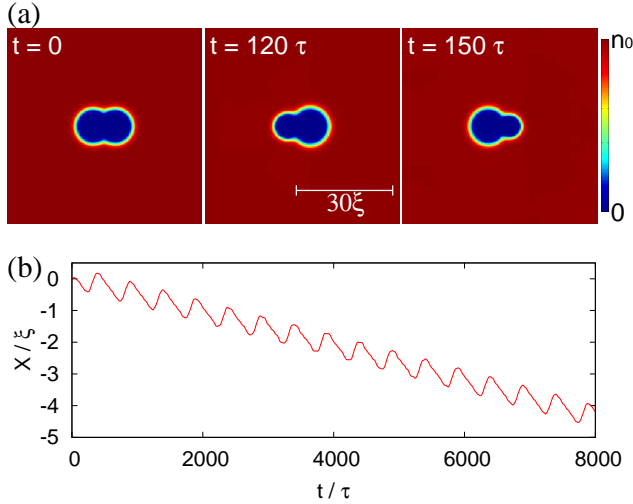


**Fig. 5.** (Color online) Time evolution of (a) the density profile  $|\psi_3|^2$  of component 3, and (b) the position  $X$  of the COM of the swimmer. See the Supplemental Material for a movie of the dynamics shown in (a).<sup>20</sup>

condition:  $g_{jk}^2 > g_{jj}g_{kk}$ , where  $j \neq k$ . They are changed as

$$g_{11} = \frac{g}{2}(1 + \tanh \gamma t \cos \omega t), \quad (15a)$$

$$g_{22} = \frac{g}{2}(1 + \tanh \gamma t \sin \omega t), \quad (15b)$$

where  $\gamma$  is introduced to avoid an initial disturbance of the system and  $g$  is a parameter that determines the units  $\xi$ ,  $v_s$ , and  $\tau$ . In the following calculation, we take  $\gamma = 0.01\tau^{-1}$  and  $\omega = 2\pi \times 0.002\tau^{-1}$ . The other interaction coefficients are fixed as follows:  $g_{33} = 1.5g$  and  $g_{12} = g_{23} = g_{13} = g$ . For  $t \gg \gamma^{-1}$ , the interaction coefficients in Eq. (15) become  $g_{11} \propto 1 + \cos \omega t$  and  $g_{22} \propto 1 + \sin \omega t$ , which do not have time-reversal symmetry.

The initial state is the ground state with  $\int |\psi_1|^2 d\mathbf{r} = \int |\psi_2|^2 d\mathbf{r} = 100n_0\xi^2$ . The density  $|\psi_3|^2$  of component 3 far from the center is  $n_0$ , a constant. The initial density profile of  $|\psi_3|^2$  is shown in the leftmost panel of Fig. 5(a), where the left and right sides of the low-density region are occupied by components 1 and 2, respectively. By changing the interaction coefficients as in Eq. (15), the shape of the swimmer deforms, as shown in Fig. 5(a). We find from Fig. 5(b) that the swimmer obtains net locomotion in the  $-x$  direction without generating waves or quantized vortices.

The locomotion of the swimmer in Fig. 5 may be understood qualitatively as follows. Suppose that the shapes of components 1 and 2 are approximated by circles with radii  $r_1$  centered at  $x_1$  and  $r_2$  at  $x_2$ , respectively, and that these circles touch each other, i.e.,

$$r_1 + r_2 = x_2 - x_1 > 0. \quad (16)$$

When component 2 expands or shrinks, component 1 is pushed or pulled as  $\dot{x}_1 \approx -\dot{r}_2$ , if the density  $n_1$  of component 1

is the same as the density  $n_3$  of the surrounding fluid of component 3. If  $n_1 > n_3$  ( $n_1 < n_3$ ), the displacement of component 1 is suppressed (enhanced), which may be approximated by  $\dot{x}_1 \approx -\dot{r}_2 + \epsilon(\bar{r} - r_1)\dot{r}_2$  to the first order of  $\bar{r} - r_1$ , where  $\bar{r}$  is the radius for which  $n_1 = n_3$  and  $\epsilon > 0$  is a constant. The same is also true when component 1 expands or shrinks, and then we have

$$\dot{x}_1 \approx -\dot{r}_2 + \epsilon(\bar{r} - r_1)\dot{r}_2 - \epsilon(\bar{r} - r_2)\dot{r}_1, \quad (17a)$$

$$\dot{x}_2 \approx \dot{r}_1 - \epsilon(\bar{r} - r_2)\dot{r}_1 + \epsilon(\bar{r} - r_1)\dot{r}_2, \quad (17b)$$

where the third terms on the right-hand side ensure Eq. (16). The motion of the COM of the swimmer thus becomes

$$\dot{X} = \frac{1}{2}(\dot{x}_1 + \dot{x}_2) \approx \frac{1}{2}(\dot{r}_1 - \dot{r}_2) - \epsilon(\bar{r} - r_2)\dot{r}_1 + \epsilon(\bar{r} - r_1)\dot{r}_2. \quad (18)$$

Assuming that  $r_1 - \bar{r} \propto \cos \omega t$  and  $r_2 - \bar{r} \propto \sin \omega t$ , the time-averaged COM in Eq. (18) becomes  $\bar{X} \propto -\epsilon\omega$ , which agrees with the fact that the swimmer travels in the  $-x$  direction in Fig. 5. It has been confirmed from numerical simulations of Eq. (14) that the time-averaged velocity  $\bar{X}$  is proportional to  $\omega$ , in agreement with the above result.

The following facts have been confirmed numerically. In a manner similar to what is shown in Fig. 4(c), the self-propulsion ceases when the swimmer stops deformation. If the change in the interaction coefficients has time-reversal symmetry, no net locomotion is obtained, due to the generalized scallop theorem. For a larger  $\omega$ , the swimmer emits excitations, in a manner similar to that shown in Fig. 3. However, in this case, components 1 and 2, that is, the body of the swimmer, are also emitted with waves and solitonic objects of component 3, and the swimmer gradually shrinks.

#### 4. Conclusions

We have investigated the dynamics of deformable objects in superfluids in order to answer the question: can we swim in a superfluid? We began by examining the dynamics of articulated bodies, as shown in Fig. 1. For a swimmer that consists of two elliptical bodies, no net locomotion is achieved when the shape of the swimmer changes sufficiently slowly (Fig. 2); this is consistent with the generalized scallop theorem. When the swimmer is deformed with a velocity comparable to or faster than the sound velocity, waves and solitonic excitations are emitted into the superfluid, and the swimmer thus acquires momentum (Fig. 3). A swimmer consisting of three elliptical bodies can swim in a superfluid without exciting waves (Fig. 4), since its motion can break time-reversal symmetry (non-reciprocal<sup>13</sup>). We next considered the dynamics of a three-component BEC, in which a swimmer comprising components 1 and 2 is surrounded by component 3. The shape of the swimmer can be changed by using the Feshbach resonance to control the interactions. We found that it is possible for such a swimmer to create self-propulsion without exciting waves; this is shown in Fig. 5. Thus, it has been shown that swimming in a superfluid can be done smoothly or with splashing.

Although, for simplicity, we have considered only uniform 2D systems, self-propulsion will also be possible in 3D superfluids. However, spatial inhomogeneity, such as in an atomic gas BEC, may hinder self-propulsion. A solution may be possible in a system with ring geometry that has rotational symmetry instead of translational symmetry; in such a system, self-propulsion may be verified by a swimmer traveling around the circumference of the ring. An interesting area for future research is to consider self-propulsion methods that are unique to quantum fluids, such as swimming by using quantized vortices or matter-wave interference.

I wish to thank T. Kiyohara for his participation in an early stage of this work. This work was supported by JSPS KAKENHI Grant Number 26400414 and by MEXT KAKENHI Grant Number 25103007.

- 1) T. B. Benjamin and A. T. Ellis, *Phil. Trans. R. Soc. Lond. A* **260**, 221 (1966).
- 2) P. G. Saffman, *J. Fluid Mech.* **28**, 385 (1967).
- 3) T. Miloh and A. Galper, *Proc. R. Soc. Lond. A* **442**, 273 (1993).
- 4) E. Kanso, J. E. Marsden, C. W. Rowley, and J. B. Melli-Huber, *J. Nonlinear Sci.* **15**, 255 (2005).
- 5) T. Chambrion and A. Munnier, *J. Nonlinear Sci.* **21**, 325 (2011).
- 6) R. J. Donnelly, A. N. Karpets, J. J. Niemela, K. R. Sreenivasan, and W. F. Vinen, *J. Low Temp. Phys.* **126**, 327 (2002).
- 7) T. Zhang, D. Celik, and S. W. Van Schiver, *J. Low Temp. Phys.* **134**, 985 (2004).
- 8) J. Jäger, B. Schuderer, and W. Schoepe, *Phys. Rev. Lett.* **74**, 566 (1995).
- 9) R. Goto, S. Fujiyama, H. Yano, Y. Nago, H. Hashimoto, K. Obara, O. Ishikawa, M. Tsubota, and T. Hata, *Phys. Rev. Lett.* **100**, 045301 (2008).
- 10) C. Zipkes, S. Palzer, C. Sias, and M. Köhl, *Nature* **464**, 388 (2010).
- 11) E. M. Purcell, *Am. J. Phys.* **45**, 3 (1977).
- 12) M. T. Reeves, T. P. Billam, B. P. Anderson, and A. S. Bradley, *Phys. Rev. Lett.* **114**, 155302 (2015).
- 13) More generally, a swimmer cannot obtain locomotion, when its motion is “reciprocal”, i.e., symmetric with respect to  $t \rightarrow -f(t)$  with  $f(t)$  being a monotonically increasing function. Periodic motion of a swimmer with one degree of freedom, such as in Fig. 1(a), is always reciprocal.
- 14) (Supplemental material) A movie of the dynamics in Fig. 2(a) is provided online.
- 15) T. Chambrion and A. Munnier, arXiv:1008.1098.
- 16) (Supplemental material) A movie of the dynamics in Fig. 3(a) is provided online.
- 17) C. A. Jones and P. H. Roberts, *J. Phys. A* **15**, 2599 (1982).
- 18) N. G. Berloff, *Phys. Rev. B* **65**, 174518 (2002).
- 19) (Supplemental material) A movie of the dynamics in Fig. 4(a) is provided online.
- 20) (Supplemental material) A movie of the dynamics in Fig. 5(a) is provided online.